Structures of Purine 2′-Deoxyribosyltransferase, Substrate Complexes, and the Ribosylated Enzyme Intermediate at 2.0 Å Resolution[†,‡]

Ruchi Anand,[§] Pierre Alexandre Kaminski,[||] and Steven E. Ealick*[,§]

Department of Chemistry and Chemical Biology, Cornell University, Ithaca, New York 14853, and Unité de Chimie Organique, URA 2128 CNRS, Institut Pasteur, Paris, France

Received September 23, 2003; Revised Manuscript Received December 10, 2003

ABSTRACT: The structure of class I *N*-deoxyribosyltransferase from *Lactobacillus helveticus* was determined by X-ray crystallography. Unlike class II *N*-deoxyribosyltransferases, which accept either purine or pyrimidine deoxynucleosides, class I enzymes are specific for purines as both the donor and acceptor base. Both class I and class II enzymes are highly specific for deoxynucleosides. The class I structure reveals similarities with the previously determined class II enzyme from *Lactobacillus leichmanni* [Armstrong, S. A., Cook, W. J., Short, S. A., and Ealick, S. E. (1996) *Structure 4*, 97−107]. The specificity of the class I enzyme for purine deoxynucleosides can be traced to a loop (residues 48−62), which shields the active site in the class II enzyme. In the class I enzyme, the purine base itself shields the active site from the solvent, while the smaller pyrimidine base cannot. The structure of the enzyme with a bound ribonucleoside shows that the nucleophilic oxygen atom of Glu101 hydrogen bonds to the O2′ atom, rendering it unreactive and thus explaining the specificity for 2′-deoxynucleosides. The structure of a ribosylated enzyme intermediate reveals movements that occur during cleavage of the *N*-glycosidic bond. The structures of complexes with substrates and substrate analogues show that the purine base can bind in several different orientations, thus explaining the ability of the enzyme to catalyze alternate deoxyribosylation at the N3 or N7 position.

N-Deoxyribosyltransferases (DRTases)[1] catalyze the transfer of a 2′-deoxyribosyl group from a donor deoxynucleoside to an acceptor nucleobase. DRTases can be divided into two classes on the basis of their substrate specificity. The DRTase I class [also called purine deoxyribosyltransferase (PTD)] is specific for the transfer of deoxyribose between two purines (Pur ↔ Pur) with the following preference for the donor substrate (*1*): deoxyinosine (dIno) > deoxyadenosine (dAdo) > deoxyguanosine (dGuo). The DRTase II class [also called nucleoside deoxyribosyltransferase (NTD)] catalyzes the transfer of deoxyribose between either purines or pyrimidines (Pur ↔ Pur, Pur ↔ Pyr, or Pyr ↔ Pyr), but has a strong preference for deoxypyrimidines as the donor substrate (*2*). The sequences of the two classes of DRTases are slightly similar (25.6% identical in *Lactobacillus helveticus*) (*1*). In the absence of an acceptor nucleobase, the DRTases display a nucleoside hydrolase activity. Both classes of DRTases are found in various *Lactobacillus* species and participate in nucleoside recycling in these microorganisms. These organisms lack purine and pyrimidine nucleoside phosphorylases, which are utilized for nucleoside recycling in most organisms, and have evolved DRTases to scavenge exogenous deoxyribonucleosides for their DNA synthesis. *Lactobacillus* species can be divided into two classes on the basis of their requirement for deoxyribonucleoside. Those species requiring a source of deoxyribonucleosides express DRTases and lack purine nucleoside phosphorylases, while those not requiring deoxynucleosides express purine nucleoside phosphorylases and lack DRTases (*1*).

To explain the existence of two deoxyribosyltransferases in *L. helveticus* and *Lactobacillus leichmanni*, it has been suggested that the specific role of PTD is the eradication of dIno from the cellular pool via conversion to hypoxanthine, which can then be recycled into inosine monophosphate by hypoxanthine phosphoribosyltransferase (*3*). Indeed, the specific activity of PTD is reported to be 20 times higher than that of NTD when dIno is the donor substrate (*1*). Another argument in favor of a specific role of PTD is the colocalization of its gene in these organisms with that of adenosine deaminase. Adenosine deaminase catalyzes the deamination of adenosine and dAdo to inosine and dIno, respectively. Thus, in the *Lactobacillus* species having a requirement for bases and deoxyribonucleosides for growth,

[†] S.E.E. is indebted to the W. M. Keck Foundation and the Lucille P. Markey Charitable Trust.

[‡] The Brookhaven Protein Data Bank entries for purine 2′-deoxyribosyltransferase are 1S2L for the native enzyme, 1S2G for the complex with dAdo, 1S3F for the complex with SeIno, 1S2I for the complex with 6-bromopurine, and 1S2D for the ribosylated intermediate.

* To whom correspondence should be addressed: Department of Chemistry and Chemical Biology, Cornell University, Ithaca, NY 14850. Telephone: (607) 255-7961. Fax: (607) 255-1227. E-mail: see3@cornell.edu.

[§] Cornell University.

[||] Institut Pasteur.

[1] Abbreviations: DRTase, *N*-deoxyribosyltransferase; NTD, nucleoside *trans*-deoxyribosylase (nucleoside 2′-deoxyribosyltransferase); PTD, purine *trans*-deoxyribosylase (purine deoxyribosyltransferase); dAdo, 2′-deoxyadenosine; dIno, 2′-deoxyinosine; SeIno, 6-selenoinosine; BrPur, 6-bromopurine; F-AraA, 2′-deoxy-2′-fluoro-β-D-arabinofuranosyladenine; Pur, purine; Pyr, pyrimidine; APS, Advanced Photon Source; MIRAS, multiple isomorphous replacement with inclusion of the anomalous scattering.

10.1021/bi035723k CCC: $27.50
Published on Web 02/11/2004

Table 1: Summary of Data Collection, Processing, and Phasing Statistics

	native	native with Hg	native with SeIno	native with dAdo	native with F-AraA	native with BrPur
resolution (Å)	2.1	3.0	2.1	2.0	2.1	2.25
wavelength (Å)	0.9794	0.9791	0.9791	0.9791	0.9791	0.9482
no. of reflections	265809	104544	453051	324335	294271	229510
no. of unique reflections	34997	12678	35106	40463	35292	28950
redundancy	7.5	8.2	13.0	8.0	8.3	7.9
completeness[a]	98.0 (100)	99.9 (100)	98.1 (100)	97.6 (99.8)	98.7 (98.6)	98.9 (98.9)
R_{sym} (%)[a,b]	5.0 (32.0)	6.2 (31.1)	6.6 (25.6)	6.8 (33.4)	5.8 (12.7)	5.5 (28.1)
I/σ[a]	8.0 (3.0)	7.7 (2.4)	6.7 (2.8)	20 (10.1)	22.0 (15.0)	20.0 (10.0)
phasing statistics						
R_{iso}[c]		27.6	25.4			
no. of heavy atom sites		3	3			
figure of merit		0.49	0.21			
phasing power[d]		1.47	0.45			

[a] Values for the outer resolution shell are given in parentheses. [b] $R_{sym} = \sum\sum_i |I_i - \langle I \rangle| / \sum \langle I \rangle$, where $\langle I \rangle$ is the mean intensity of the N reflections with intensities I_i and common indicies h, k, and l. [c] $R_{iso} = ||F_{PH}| - |F_P||/|F_P|$, where F_P and F_{PH} are the structure factor amplitudes for the native and derivative crystals, respectively. [d] Phasing power $= \langle F_H/E \rangle$, where F_H is the heavy atom structure factor and E is the lack of closure error.

in the absence of PTD, dIno would not be catabolized efficiently by NTD alone.

The transferase reaction catalyzed by DRTase proceeds via a ping-pong−bi-bi mechanism (*4*) and involves the formation of a deoxyribosyl−enzyme intermediate. The stereospecificity of the glycosyl transfer, which results in formation of only the β anomer of the nucleoside, has been exploited in synthesizing a large number of nucleoside analogues. Of particular interest are 2-halo-2′-deoxypurine nucleosides (*5*) and 2′,3′-dideoxynucleosides, which have implications in the treatment of AIDS and cancers (*6*, *7*). Previous studies revealed that an active site glutamic acid residue serves as the attacking nucleophile (*8*). The deoxyribosyl transferase reaction is mechanistically similar to the double displacement reaction identified in the retaining class of glycoside hydrolases that catalyze analogous reactions with retention of stereochemical configuration and also utilize the carboxyl group from a glutamyl or an aspartyl residue as the active site nucleophile (*9*, *10*).

The structure of *L. leichmanni* NTD (PDB entry 1F8X) was previously determined to 2.5 Å resolution (*11*). The structure showed that NTD is a hexamer in its native state and is composed of identical ~18 kDa subunits. The monomer fold is a single double-wounded α/β domain composed of a five-stranded β-sheet flanked by four helices. Although there is one active site per subunit, each complete catalytic center requires participation from a neighboring subunit, and the hexameric enzyme packs as a trimer of dimers.

In this study, we determined the structure of PTD from *L. helveticus* to 2.0 Å resolution, alone and complexed with various ligands. The rarity of PTD, as well as its low level of sequence homology with other known proteins, made it an attractive target for structure determination. The ribosylated, esterified PTD intermediate was also prepared and crystallized in an effort to better understand the structural mechanism. The question of the specificity of NTD and PTD toward 2′-deoxynucleosides was addressed by determining the structure of 6-selenoinosine (SeIno) complexed with PTD. The structure of 6-bromopurine (BrPur) complexed with PTD was also determined to examine the tendency of DRTases to transfer the deoxyribosyl group to the N3 or N7 position of the acceptor purine base instead of to the usual N9 position (*12*, *13*).

MATERIALS AND METHODS

Crystallization of PTD. PTD was purified as previously described (*1*). The purified protein was buffer exchanged into 20 mM MES (pH 8.0) and concentrated to 20 mg/mL using an Amicon micron centrifugal concentrator. Initial crystallization conditions for native PTD were determined using the sparse matrix screens, Crystal Screen 1 and Crystal Screen 2 (Hampton Research). Several conditions yielded crystals that varied in quality, and the optimized conditions were found to be 2.0 M ammonium sulfate and 100 mM Tris (pH 8.0). The crystals were grown at room temperature using the hanging-drop vapor diffusion technique. Drops (4 μL) containing a 1:1 mixture of protein and reservoir solutions were optimal for crystal growth. Diffraction quality crystals grew over a period of 4−7 days. Under these conditions, PTD crystallizes in the tetragonal space group $P4_32_12$ with the following unit cell dimensions: $a = 80.7$ Å and $c = 186.2$ Å. Each asymmetric unit contains three monomers corresponding to a calculated solvent content of 60%. 2′-Deoxyadenosine, BrPur, SeIno, and 2′-deoxy-2′-fluoro-β-D-arabinofuranosyladenine (F-AraA) were soaked into the crystals at concentrations of 2−5 mM for approximately 24 h. A mercury derivative of PTD was prepared by soaking PTD crystals in 100 μM methylmercury benzoate.

Data Collection and Processing. The native and derivative data sets were collected at NE-CAT beamline 8-BM at the Advanced Photon Source (APS) using a Quantum 315 detector (Area Detector Systems Corp.) in the binned format. A cryoprotectant solution of 20% glycerol in the mother liquor was used to prevent damage during freezing. An X-ray absorption spectrum in the vicinity of the Se K-absorption edge was determined for the PTD−SeIno complex crystal by recording the X-ray fluorescence as a function of wavelength. Diffraction data were then collected at the peak of the spectrum (0.9791 Å), for both the SeIno and Hg derivatives. The data were measured in 1° oscillations with 10 s exposure times, with a crystal to detector distance of 300 mm. To minimize systematic errors, Bijovet pairs were acquired close in time by collecting the data in 5° wedges followed by a wedge having inverse beam geometry (ϕ + 180°). A total of 90° of data were collected for each set. The DENZO suite of programs was used for integration and scaling of the data (*14*). Final data processing statistics are shown in Table 1.

Table 2: Final Refinement Statistics

	native	native with SeIno	native with dAdo	native with F-ArA	native with BrPur
resolution (Å)	25−2.1	25−2.3	25−2.0	25−2.1	25−2.3
no. of non-hydrogen atoms	4054	4013	4135	4198	4059
no. of protein atoms	3763	3794	3709	3863	3845
no. of water molecules	291	162	272	281	184
no. of ligand atoms	−	57	54	54	30
no. of reflections in refinement	33508	55196	33646	34823	28333
no. of reflections in test set	3334	5432	3367	3471	2818
R-factor (%)[a]	22.7	23.3	22.8	22.8	22.5
R_{free} (%)[b]	27.3	27.4	26.9	25.7	26.9
rms deviation from ideal geometry					
bonds (Å)	0.006	0.006	0.006	0.008	0.008
angles (deg)	1.24	1.23	1.23	1.34	1.35

[a] *R*-factor $= \sum_{hkl}||F_{obs}| - k|F_{calcd}||/\sum_{hkl}|F_{obs}|$, where F_{obs} and F_{calcd} are observed and calculated structure factors, respectively. [b] R_{free} is calculated over a subset of reflections (10%) excluded from all stages of refinement.

MIRAS Phasing. The selenium and mercury atom positions were determined using SnB (*15*−*17*), which utilizes the Shake-and-Bake dual space direct methods of Hauptman and co-workers. The DREAR suite of programs (*18*) was used to calculate the normalized anomalous differences (ΔE) to 3.0 Å resolution in the case of mercury and to 2.5 Å resolution in the case of selenium. Three mercury and three selenium positions corresponding to each monomer in the asymmetric unit were found. These sites were used to define the noncrystallographic 3-fold axis. The mercury and selenium positions were input into CNS (*19*). Isomorphous and anomalous differences for both mercury and selenium were used for phasing. The initial map was further averaged using noncrystallographic symmetry (NCS) in the RAVE suite of programs (*20*).

Model Building and Refinement. All model building for native PTD was performed using the computer program O (*21*). The Cα trace was built through clear stretches of electron density at 3.0 Å resolution for the monomer, and two additional subunits were generated using NCS. The side chains were then included where possible and left as polyalanine for the rest of the model. Successive rounds of rigid body refinement, simulated annealing, temperature factor refinement, and model building in conjunction with phase extension to 2.1 Å enabled the tracing of all 167 amino acid residues. The NCS constraints were kept on for initial rounds of refinement and were slowly relaxed and finally removed in the final round. Water molecules were included in subsequent rounds of refinement based on the criteria that the peak in difference electron density maps was greater than 3σ and the water molecule formed at least one hydrogen bond with a protein, ligand, or solvent atom.

The structure of native PTD was used as a molecular replacement model in determining the structures of all PTD complexes. The PTD complexes were refined using a similar minimization and fitting cycle as described above for the unliganded PTD structure. The standard topology, link, and parameter files in CNS were modified to include the definition of a ribosylated glutamate residue for describing Glu101. The final data refinement statistics are presented in Table 2.

RESULTS

Unliganded PTD. The three-dimensional structure of PTD (Figure 1) was determined by using two derivatives with inclusion of the anomolous scattering signal for both mercury and selenium. There are three molecules in the asymmetric unit related by a noncrystallographic 3-fold axis. The main chain atoms for all 167 residues in PTD were traced, but no side chain atoms could be built for residues 1−4. The overall structure of PTD is very similar to the previously determined structure of NTD (*11*). PTD, like NTD, is a hexamer in which the monomer consists of a central core structure with a five-stranded parallel β-sheet, flanked by four helices. The major differences between PTD and NTD are in the loop regions. A superposition of 95 residues of PTD with NTD using PROFIT (*22*) gave an rms deviation of 1.7 Å. The major structural difference is a 12 Å shift of the loop of residues 48−62 in PTD, near the active site, which corresponds to residues 46−60 in NTD. This difference results in an active site volume for PTD of 411.9 Å^3 compared to a volume of 220.1 Å^3 in NTD (*23*). Other loops that show significant structural differences include residues 119−125 in PTD, which correspond to residues 116−120 in NTD, and a loop comprising residues 16−20, which correspond to residues 13−16 in the NTD structure.

2′-Deoxyadenosine Complex. In the PTD−dAdo complex, the nucleoside is clear in the $F_o - F_c$ density at a contour level of 3σ (Figure 2A). The deoxyribosyl moiety is tightly anchored through hydrogen bonding between the O5′ atom and the OD1 and OD2 atoms of Asp75, with distances of 2.82 and 2.64 Å, respectively. The O5′ atom also hydrogen bonds to the OD1 atom of Asn128# from the neighboring subunit with a distance of 2.66 Å. The O3′ atom is anchored in position by the OE1 atom of Glu101 and the backbone nitrogen atom of Ser14, with hydrogen bonding distances of 2.50 and 3.06 Å, respectively. The adenine base is held in position by hydrogen bonding interactions between N3 and the OD2 atom of Asp75 and the N7 atom and a C-terminal oxygen atom of Tyr167#-COOH, with distances of 2.62 and 2.85 Å, respectively. The N6 atom hydrogen bonds to a water molecule with a distance of 2.75 Å. Phe45, which is disordered in the native PTD structure, makes a π-stacking interaction with the adenine ring.

Ribosylated PTD Intermediate. An $F_o - F_c$ map contoured at 3.4σ showed that in the structure of PTD treated with F-AraA, the *N*-glycosidic bond is broken and the 2′-fluoroarabinose is covalently bound to the OE2 atom of Glu101 (Figure 2B). The ribosyl group in the ester intermediate retained the O4′-*exo* sugar pucker observed in the PTD−dAdo complex structure. The sugar position is shifted

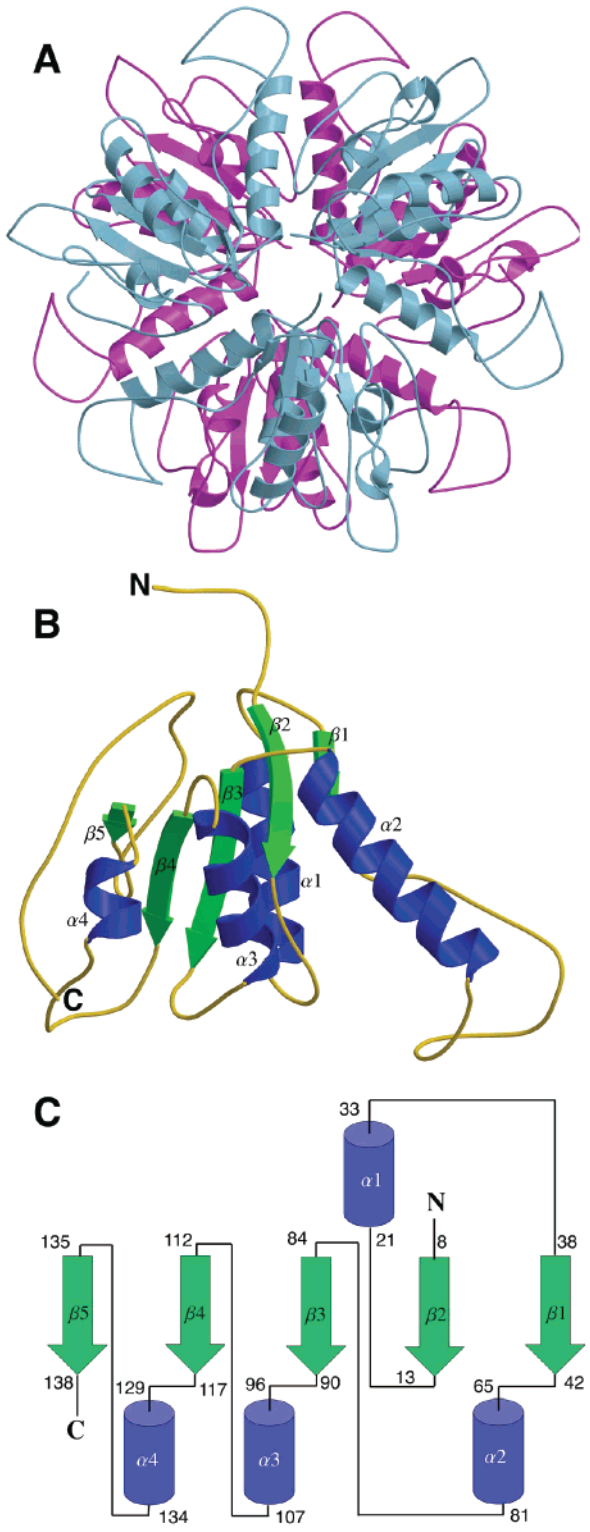

FIGURE 1: (A) Structure of the hexamer of PTD. Each functional dimer consists of a bottom (magenta) and a top (blue) monomer. (B) Monomeric structure of PTD. (C) Topology diagram of PTD. This figure was prepared using MOLSCRIPT (*26*) and Raster3D (*27*, *28*).

toward Glu101 by approximately 1.3 Å for formation of the covalent bond, while the position of the adenine base remains fixed. In the ribosylated PTD intermediate, the O5′ atom remains anchored in position by Asp95 and shows almost no movement relative to the PTD−dAdo complex. The O5′ atom gains a hydrogen bond to the hydroxyl oxygen atom of Tyr17 relative to the dAdo complex. This tyrosine is on a flexible loop that becomes ordered during the formation of the intermediate. The O3′ atom moves slightly closer to the backbone nitrogen of Ser14 and hence forms a tighter hydrogen bond. The carboxylate group of Glu101 moves closer to the sugar in the intermediate structure so that the O3′ atom of the sugar is within hydrogen bonding distance (2.63 Å) of the OE1 atom of Glu101. In the process, Glu101 loses the hydrogen bonding interaction with Tyr11, which was present in the substrate-bound complex. The major movement of the sugar ring occurs in the C2′ and O4′ atoms, which are not involved in hydrogen bonding interactions in either the PTD−dAdo complex or the intermediate and C1′, which form a covalent bond with the OE2 atom of Glu101.

The ribosylated PTD intermediate also shows clear density in an $F_o - F_c$ map for the cleaved adenine base. In this case, the adenine base is flipped in the active site such that N1, rather than N3, is hydrogen bonded to Asp75. In addition, the OE1 oxygen of Asp75 is within hydrogen bonding distance (2.92 Å) of the N6 atom of the base. The N6 atom is also 3.10 Å from a water molecule, which in turn is 3.15 Å from the backbone oxygen of Gly44.

PTD−SeIno Complex. The structure of the PTD−SeIno complex shows that the nucleoside is shifted away from attacking nucleophile Glu101 with respect to the substrate dAdo. The sugar pucker for SeIno is C2′-*endo* instead O4′-*exo* as observed for the substrate and intermediate complexes. The distance from the C1′ atom to the OE2 atom of Glu101, in the case of SeIno, is 4.0 Å as compared to 3.2 Å for dAdo. The N7 position of the base is still anchored by the carboxylate oxygen atom of the terminal Tyr167#-COOH from the neighboring subunit, which is 2.8 Å away, and the O5′ atom is anchored by OD1 and OD2 of Asp95, which are 2.8 and 2.6 Å away, respectively. However, the hydrogen bond with Asp128 from the adjacent residue is no longer present in this complex, and Asp75 hydrogen bonds to the O2′ atom of SeIno instead of hydrogen bonding with the N3 atom of the base, as in the case of the substrate, dAdo. The O2′ atom also hydrogen bonds to the OE2 atom of Glu101 and Tyr11 with hydrogen bonding distances of 2.5 and 3.1 Å, respectively. Tyr11 also hydrogen bonds the OE2 atom of Glu101; however, this distance, which was 2.6 Å in the dAdo complex, has now increased to 3.1 Å in the SeIno complex. The O3′ atom is still anchored in place by the OE1 atom of Glu101.

PTD−BrPur Complex. The BrPur complex structure shows density for the base at a contour level of 3.2σ in an $F_o - F_c$ map. Compared to the PTD−dAdo substrate complex, the base has rotated by approximately 90° in the active site such that N7 now occupies the normal position of N3 and the OD1 carboxylate of Asp75 is now within hydrogen bonding distance (2.7 Å) of the N7 atom. The plane of the adenine base remains the same, and π-stacking interactions with Phe45 are retained. The N9 and N3 positions are hydrogen bonded to a structurally ordered water molecule. The bromine in position 6 is facing the active site cleft and is 3.8 Å from Tyr17.

DISCUSSION

Mechanistic Implications. PTD and NTD catalyze the transfer of a 2′-deoxyribosyl group from a nucleoside and an acceptor nucleobase. Previous mechanistic studies show

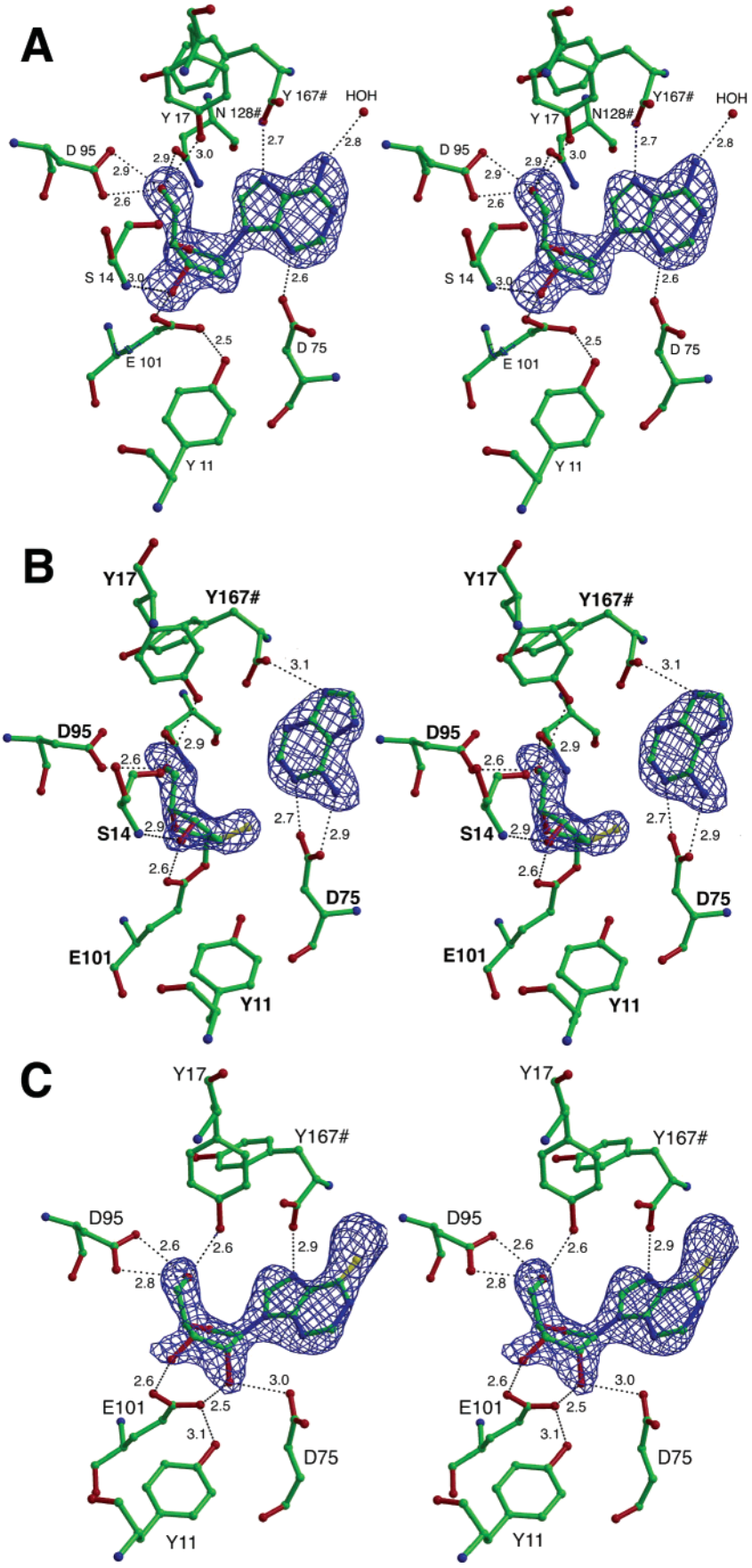

that the reaction proceeds via a ping-pong−bi-bi mechanism involving a covalent deoxyribosyl−enzyme intermediate and results in retention of the anomeric configuration of the nucleoside product (*4*). The deoxyribosyl transfer is mechanistically similar to the double displacement reaction identified for the retaining class of glycoside hydrolases (*10*). In the case of PTD, Glu101 serves as an active site attacking nucleophile. The crystal structure of PTD complexed with

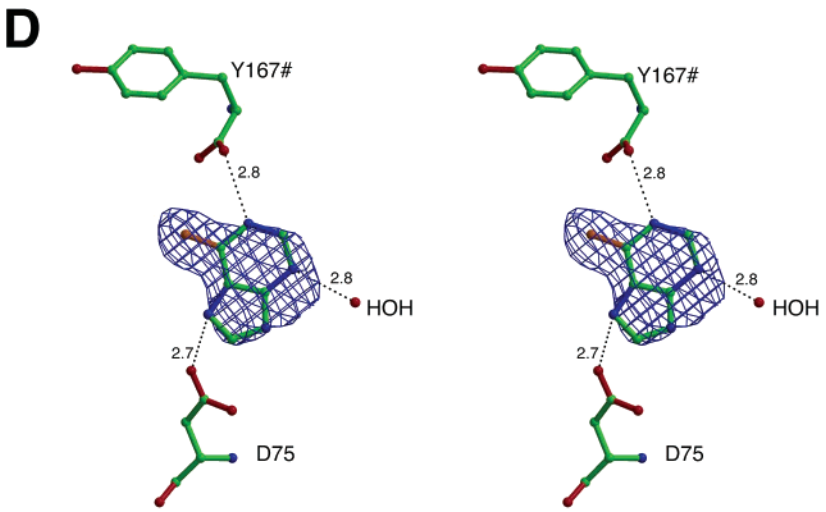

FIGURE 2: Stereoview of the active site of PTD. (A) The $F_o - F_c$ density for the substrate dAdo is shown contoured at 3.1σ. (B) The $F_o - F_c$ density for the ribosylated ester intermediate covalently bound to Glu101 is shown contoured at 3.4σ. (C) The $F_o - F_c$ density for selenoinosine is shown contoured at 2.9σ. (D) The $F_o - F_c$ density for bromopurine is shown contoured at 3.0σ. This figure was prepared using BOBSCRIPT (*29*, *30*) and Raster3D (*27*, *28*).

dAdo reveals several structural features that are consistent with the proposed mechanism.

The deoxynucleoside is oriented for catalysis by several hydrogen bonds. In the PTD−dAdo complex, the C1′ atom is 3.2 Å from the OE2 atom of Glu101 with a nearly ideal trajectory for attack. The deoxyribose is oriented by two strong hydrogen bonds from O5′ to Asp75 and an additional hydrogen bond from O5′ to Asn128# of a neighboring subunit. The O3′ atom is hydrogen bonded to one carboxylate oxygen atom of Glu101, while the other oxygen atom serves as the nucleophile. The positioning of the carboxylate group by O3′ of the sugar is reminiscent of the way the phosphate nucleophile is positioned by O3′ in purine nucleoside phosphorylase (*24*, *25*). The attachments to O3′ and O5′ create an anchor about which the ribosyl group pivots during the cleavage and formation of the *N*-glycosyl bond.

The cleavage of the N9−C1′ glycosidic bond most likely occurs via an oxocarbenium-like transition state in which negative charge accumulates on the purine ring and positive charge accumulates on the C4′−O4′ bond of the sugar. The C-terminal carboxylate group of Tyr167# of an adjacent monomer is positioned to protonate N7. This is consistent with site-directed mutagenesis studies that show negligible transferase activity when Tyr167 is truncated (*8*). An only 40% loss of activity is observed for the Y167F mutant, demonstrating that it is the C-terminal carboxylate rather than the side chain that is necessary for catalysis. The delocalization of the negative charge in the purine ring may be further assisted by protonation of the N3 atom by Asp75. Mutation of Asp75 to alanine results in a 100-fold loss of activity (*8*). Both of these active site carboxylate residues are proposed to be protonated. They are surrounded by hydrophobic residues, including Phe45, Phe16, Phe43, Tyr11, Try16, Trp67, and Met125, and thus, the local pK_a is likely to be shifted upward.

The sugar pucker also facilitates deoxynucleoside bond cleavage. In the PTD−dAdo complex, the dAdo adopts a high-energy O4′-*exo* pucker. This sugar pucker places the C1′ atom above the plane defined by C2′, O4′, and C4′. As the *N*-glycosidic bond begins to stretch during bond cleavage, the C1′ atom moves into the C2′−O4′−C4′ plane, satisfying the planarity requirement of the oxocarbenium transition state. If the sugar pucker places C1′ in or below the plane, stretching of the glycosidic bond conflicts with creation of a planar intermediate.

Ribosylated Enzyme Intermediate. 2′-Deoxy-2′-fluoroglycosides with a good leaving group at position 1′ are slow alternative substrates for numerous glycosidases. After the loss of the leaving group, the electron-withdrawing fluorine atom at position 2′ of the sugar favors the covalently bound intermediate and destabilizes the oxocarbenium-like transition state. In many cases, the 2′-deoxy-2′-fluoroglycopyranosyl−enzyme intermediate accumulates, thus inactivating the enzyme (*10*). The stability of these intermediates with β-glucosidase, β-galactosidase, *exo*-1,4-glucanase, *endo*-β-14-glucanase, and β-1,4-xylanase is so high that a proteolytic digest of the inhibited enzyme yields a peptide fragment containing a modified glutamyl residue. In the case of NTD from *L. leichmanni*, a covalently modified enzyme intermediate was isolated using treatment with a 2′-fluoronucleoside followed by hydrolysis (*2*). We used a similar strategy to inactivate PTD and determine the crystal structure of the ribosylated enzyme intermediate. The key interactions of the ribosylated enzyme intermediate are shown in Figure 2B.

The crystal structures of the PTD−dAdo complex and the ribosylated enzyme intermediate provide two snapshots along the reaction coordinate. Comparison of these structures suggests that the carboxylate OE1 atom of Glu101 is anchored by a hydrogen bond with the O3′ atom of the sugar. As the reaction proceeds, the OE2 atom of Glu101 pivots by approximately 55° about the anchored OE1 atom and attacks the C1′ atom of the nucleoside substrate. The movement of the carboxylate OE2 atom results in the loss of a hydrogen bond with the phenolic oxygen atom of Tyr11. Tyr11 then donates a new hydrogen bond to Asp75, which if protonated donates a hydrogen bond to N3 of the purine base. Once the glycosidic bond begins to stretch, an oxocarbenium ion forms and is trapped by Glu101, resulting in inversion of configuration at C1′. Both the O5′ position and O3′ position of the sugar are tightly anchored and undergo very little movement, while the major movement of the ribosyl moiety occurs at the C1′, O4′, and C2′

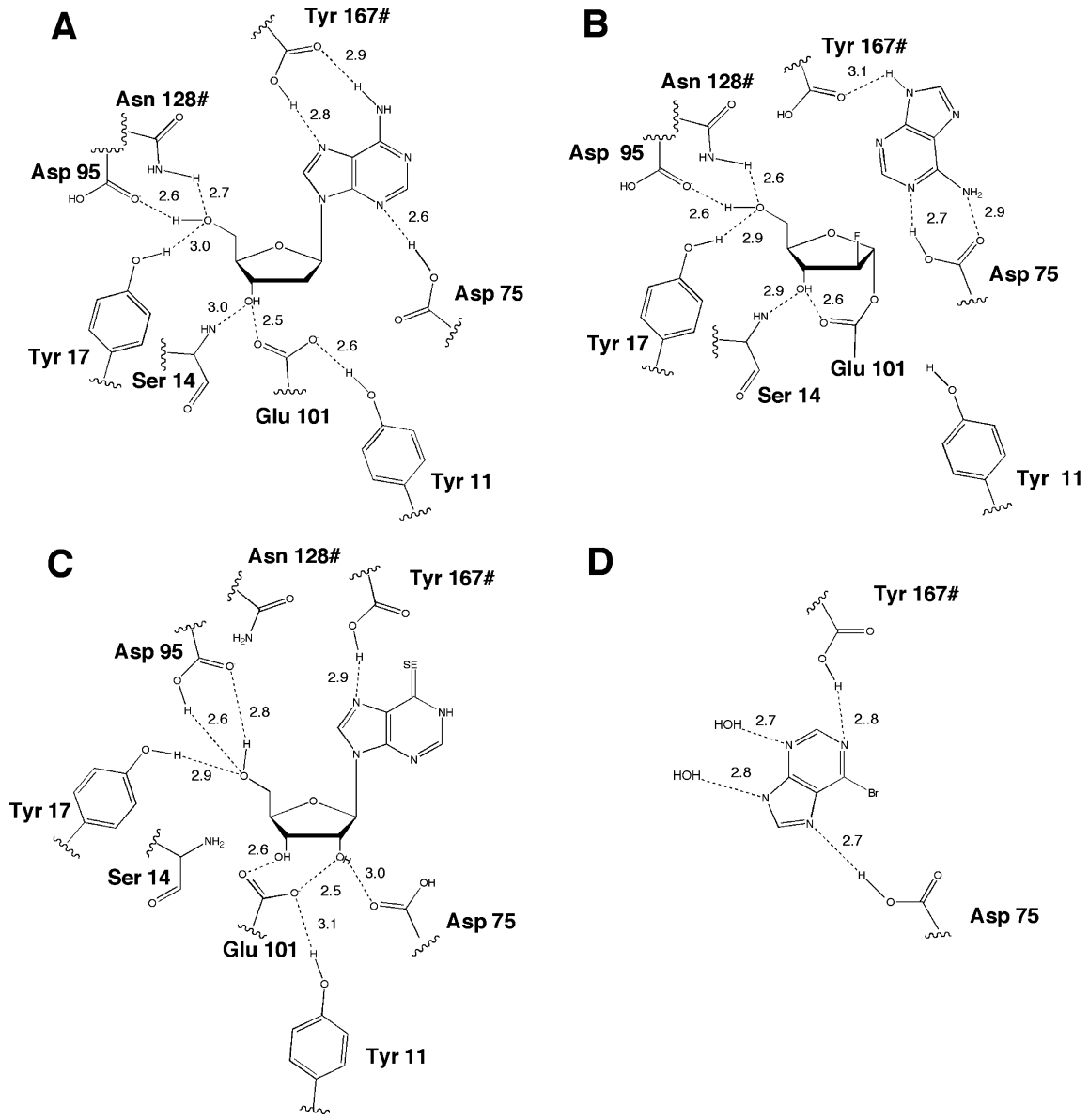

FIGURE 3: PTD active site with bound ligands. Key active site residues and hydrogen bonding patterns are shown for complexes with (A) dAdo, (B) ribosylated intermediate and adenine, (C) SeIno, and (D) BrPur.

positions. Like the substrate nucleoside, the enzyme-bound ribose also has a strained O4′-*exo* conformation.

Specificity of PTD for 2′-Deoxyribose. Although PTD and NTD accept most naturally occurring nucleosides as well as many with modified bases, the enzymes are highly specific for 2′-deoxyribosyl groups. A comparison of the PTD−dAdo and PTD−SeIno structures provides an explanation for the specificity of these enzymes for 2′-deoxynucleosides (Figure 3). While the PTD−dAdo complex shows good geometry for catalysis, the PTD−SeIno complex shows important differences in hydrogen bonding patterns. The presence of a hydroxyl group at the C2′ position results in hydrogen bonds to both carboxylate oxygen atoms of Glu101. O3′ shows the normal hydrogen bond, but O2′ of the sugar now hydrogen bonds to the carboxylate oxygen atoms that serves as the nucleophile. To accommodate the additional hydroxyl group into the active site of PTD, SeIno moves farther away from Glu101 with a distance between the C1′ atom of the sugar and the carboxylate OE2 atom of 4.0 Å. The shift of the SeIno molecule also results in the loss of the interaction with Asp75, which now forms a hydrogen bond with the O2′ atom of the sugar. Thus, the presence of the sugar O2′ atom not only occludes the active site nucleophile but also destabilizes the transition state by breaking a key hydrogen bonding interaction. The loss of interactions to the purine base also shows up in the *B*-factor analysis of the two compounds. The *B*-factor of dAdo is 21 Å^2, which is lower than the average *B*-factor value of 30 Å^2 for the enzyme, while the *B*-factor for SeIno is 42 Å^2, which is substantially higher than that of the enzyme. Finally, the sugar pucker in the case of SeIno is C2′-*endo*. This sugar conformation is both energetically more favorable than O4′-*exo* and, for the reasons given above, stereochemically unfavorable for catalysis.

Specificity of PTD for Purine Nucleosides. Unlike NTD, which utilizes both purine and pyrimidine donors and acceptors, PTD is highly specific for 2′-deoxynucleosides with purine bases. Comparison of the structures of PTD and NTD shows that although the overall core is conserved, there are structural differences that may account for the differences in specificity. Figure 4 shows the differences in Cα positions when NTD is superimposed on PTD. The plot shows two

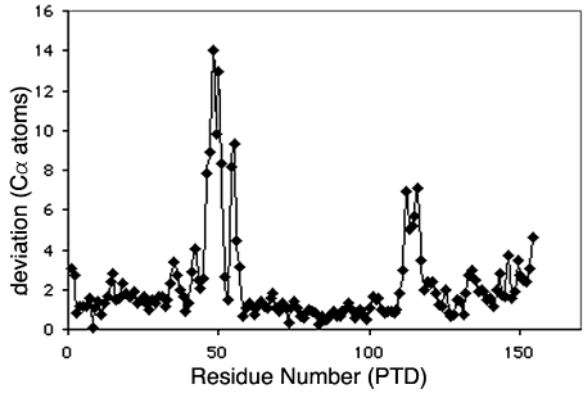

FIGURE 4: Comparison of the Cα atom positions of PTD and NTD. The PTD residue numbers are plotted on the *x*-axis, and the difference in the Cα positions of NTD and PTD is plotted on the *y*-axis. The superposition was based on 93 Cα atoms with an rms deviation of 0.97 Å.

distinct regions that have significant differences between the two structures. The first region spans the loop region in PTD (residues 48−62), which serves as an active site flap. In the case of NTD, this loop contains Gln46, one of the key active site residues which hydrogen bonds to both purine and pyrimidine bases. This stabilizing interaction is lost in the case of PTD because the equivalent residue is a glycine residue. In the case of NTD, this loop closes over the opening of the active and thus shields it from the surrounding environment. However, in the case of PTD, this loop adopts a conformation that leaves an approximately 12 Å opening compared to NTD. Binding of purine nucleosides results in active site shielding; however, the smaller pyrimidine base does not.

The substrate binding geometry and key active site residues apart from the 48−62 loop are very similar in both enzymes (Figure 5A). Figure 5B shows the superposition of the active site residues of NTD and PTD. Both active sites are lined with three acidic residues, which are implicated in substrate binding and catalysis. This hydrophilic core is shielded by a shell of hydrophobic residues, including tryptophan, methionine, tyrosine, and phenylalanine. Although both enzymes have this hydrophobic shell, there are some subtle differences between the two enzymes in this region. In most nucleoside binding enzymes, the nucleoside base is stabilized by a π-stacking interaction. In the case of PTD, Phe45 stacks next to the purine nucleoside base and is present on a flexible loop that becomes ordered on substrate binding. Phe45 is further positioned for a face-to-face interaction with the purine base by other hydrophobic residues, including Phe16, Phe43, and Tyr17. However, in the case of NTD, Trp12, which aligns with Phe16 in PTD, makes an edge-on

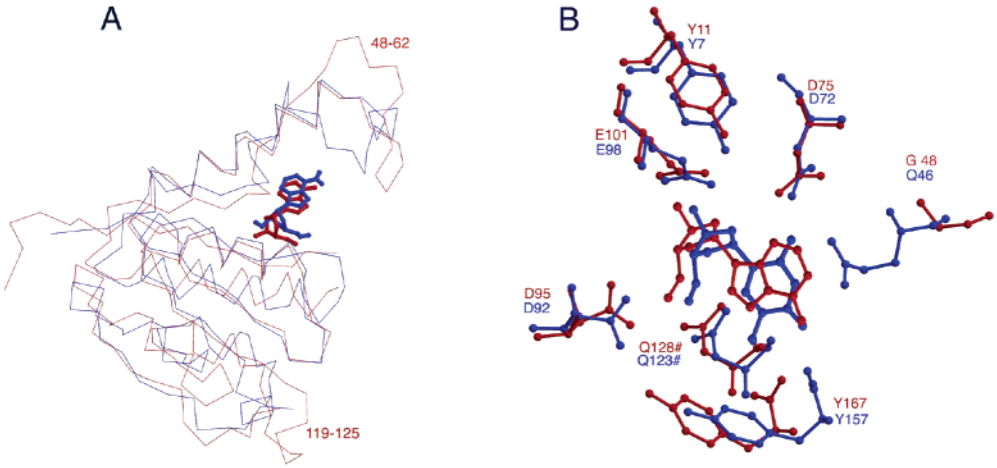

FIGURE 5: Comparison of the structures of PTD and NTD. (A) Superposition of the Cα tracings of PTD (red) and NTD (blue). (B) Comparison of the active site residues of PTD (red) and NTD (blue). The pseudouridine molecule is from the NTD structure.

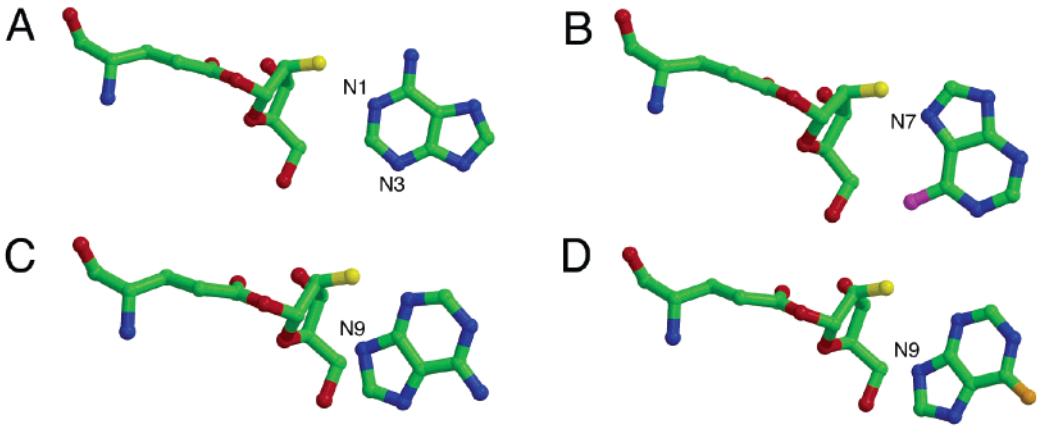

FIGURE 6: Different orientations of the purine base in the PTD active site. The four panels show the purine base and hydrogen bonding schemes for (A) the ribosylated intermediate with bound adenine, (B) 6-bromopurine, (C) deoxyadenosine, and (D) 6-selenoinosine. Panels B−D show the ribosylated intermediate from panel A for reference. This figure was prepared using MOLSCRIPT (*26*) and Raster3D (*27*, *28*).

interaction with the purine base. Thus, the angle of the π-stacking interaction is more favorable in PTD than in NTD. This suggests that base stacking is more critical in PTD, and is able to compensate for the missing glutamine residue, which hydrogen bonds to both purines and pyrimidines in the active site of NTD. The π-stacking interaction in the case of PTD, primarily through Phe45, would likely position the pyrimidine base too far from the C1′ atom of the covalently bound ribosyl intermediate for attack.

The second major difference between PTD and NTD is the loop that spans residues 119−125 in PTD. The equivalent loop consists of residues 116−120 in NTD. This hydrophilic loop may serve as an anchor for the C-terminal region of the enzyme which contains the catalytically important C-terminal Tyr167#-COOH. The positioning of the C-terminus may be more critical for the purine specific PTD than for NTD.

N3 and N7 Ribosylation Reactions. One unusual feature of this class of enzymes is their ability to transfer the deoxyribose moiety to the N7 or N3 atom of the purine base instead of the usual N9 position (*12*, *13*). The collection of structures reported here shows purine bases in the three different orientations, each consistent with one of the known deoxyribosyl transfer reactions. A comparison of the positions of the bases in the three structures, substrate dAdo, cleaved base in F-AraA, and BrPur, shows that the base is primarily held in the active site by its hydrogen bonding interaction with Asp75, Tyr167#-COOH, and the π-stacking interaction with Phe45.

The three structures show that the enzyme can bind the purine base at the active site in more than one orientation (Figure 6). In the case of the normal substrate 2′-deoxyadenosine, the base is positioned by hydrogen bonding interactions of N3 and N7 atoms, which hydrogen bond to Asp75 and Tyr167#-COOH, respectively. This orients the purine base for attack at the N9 position. The base of the unreactive SeIno complex is in a similar orientation. However, in the case of the 6-bromopurine complex, the base is rotated in plane approximately 90° with respect to the adenine base of 2′-deoxyadenosine and now the N7 and N1 atoms make hydrogen bonds with Asp75 and Tyr167#-COOH, respectively. To further stabilize this orientation, the N3 and N9 atoms make hydrogen bonds with water molecules. Thus, in the case of BrPur, the base is oriented with N7 positioned for attack, with a predicted distance to the C1′ atom of 4.0 Å. In the case of the F-AraA complex, the N1−C1′ glycosidic bond is cleaved and the base is reoriented such that N1 and N3 are closest to the C1′ atom. The base is oriented by hydrogen bonding interactions of N1 and N6 atoms with Asp75. The N9 atom also hydrogen bonds to the carboxylate oxygen atom of Tyr167#-COOH. The presence of a 2′-fluoro substituent on the ribose sugar may affect the geometry; however, the N3 atom is approximately in position for attack at C1′.

In all three orientations, the plane of the purine base is approximately the same, and the different orientations are achieved by rotations about the normal to the plane. These different orientations place either N9, N3, or N7 near the C1′ atom and provide hydrogen bond donors to stabilize the negative charge that accumulates on the purine base during catalysis. The binding of the deoxyribose, however, has only one possible conformation, which is dictated by hydrogen bonds to Ser14, Tyr17, Asp95, Glu101, and Asn128#. Thus, although the PTD is highly selective for purine deoxynucleosides, the transfer of the deoxyribosyl moiety can occur at several positions on the purine base.

REFERENCES

1. Kaminski, P. A. (2002) Functional cloning, heterologous expression, and purification of two different N-deoxyribosyltransferases from *Lactobacillus helveticus*, *J. Biol. Chem. 277*, 14400−14407.
2. Porter, D. J., Merrill, B. M., and Short, S. A. (1995) Identification of the active site nucleophile in nucleoside 2-deoxyribosyltransferase as glutamic acid 98, *J. Biol. Chem. 270*, 15551−15556.
3. Beardsley, S. K. S., and Greenbaum, A. L. (1988) Enzymes of the pathway of purine synthesis in the rat mammary gland. Changes in the lactation cycle and the effects of diabetes, *Biochem. J. 250*, 395−399.
4. Danzin, C., and Cardinaud, R. (1974) Deoxyribosyl transfer catalysis with trans-N-deoxyribosylase. Kinetic studies of purine-to-purine trans-N-deoxyribosylase, *Eur. J. Biochem. 48*, 255−262.
5. Huang, M. C., Hatfield, K., Roetker, A. W., Montgomery, J. A., and Blakley, R. L. (1981) Analogs of 2′-deoxyadenosine: facile enzymatic preparation and growth inhibitory effects on human cell lines, *Biochem. Pharmacol. 30*, 2663−2671.
6. Carson, D. A., and Wasson, D. B. (1988) Synthesis of 2′,3′-dideoxynucleosides by enzymatic trans-glycosylation, *Biochem. Biophys. Res. Commun. 155*, 829−834.
7. Freeman, G. A., Shaver, S. R., Rideout, J. L., and Short, S. A. (1995) 2-Amino-9-(3-azido-2,3-dideoxy-β-D-erythro-pentofuranosyl)-6-substituted-9H-purines: synthesis and anti-HIV activity, *Bioorg. Med. Chem. 3*, 447−458.
8. Short, S. A., Armstrong, S. R., Ealick, S. E., and Porter, D. J. (1996) Active site amino acids that participate in the catalytic mechanism of nucleoside 2′-deoxyribosyltransferase, *J. Biol. Chem. 271*, 4978−4987.
9. MacLeod, A. M., Lindhorst, T., Withers, S. G., and Warren, R. A. (1994) The acid/base catalyst in the exoglucanase/xylanase from *Cellulomonas fimi* is glutamic acid 127: evidence from detailed kinetic studies of mutants, *Biochemistry 33*, 6371−6376.
10. McCarter, J. D., and Withers, S. G. (1994) Mechanisms of enzymatic glycoside hydrolysis, *Curr. Opin. Struct. Biol. 4*, 885−892.
11. Armstrong, S. R., Cook, W. J., Short, S. A., and Ealick, S. E. (1996) Crystal structures of nucleoside 2-deoxyribosyltransferase in native and ligand-bound forms reveal architecture of the active site, *Structure 4*, 97−107.
12. Holguin-Hueso, J., and Cardinaud, R. (1972) Enzymic synthesis of 9- and 7-(2′-β-D-deoxyribosyl)xanthine, *FEBS Lett. 20*, 171−173.
13. Huang, M. C., Montgomery, J. A., Thorpe, M. C., Stewart, E. L., Secrist, J. A., III, and Blakley, R. L. (1983) Formation of 3-(2′-deoxyribofuranosyl) and 9-(2′-deoxyribofuranosyl) nucleosides of 8-substituted purines by nucleoside deoxyribosyltransferase, *Arch. Biochem. Biophys. 222*, 133−144.
14. Otwinowski, Z., and Minor, W. (1997) Processing of X-ray diffraction data collected in oscillation mode, *Methods Enzymol. 276*, 307−326.
15. Hauptman, H. A. (1991) A minimal principle in the phase problem, in *Crystallographic Computing 5: From Chemistry to Biology* (Moras, D., Podnarny, A. D., and Thierry, J. C., Eds.) pp 324−332, IUCr and Oxford University Press, Oxford, U.K.
16. Miller, R., DeTitta, G. T., Jones, R., Langs, D. A., Weeks, C. M., and Hauptman, H. A. (1993) On the application of the minimal principle to solve unknown structures, *Science 259*, 1430−1433.
17. Weeks, C. M., and Miller, R. (1997) in *Proceedings of the Macromolecular Crystallography Computing School* (Bourne, P., and Watenpaugh, K., Eds.) pp 138−147, Macromolecular Crystallography Computing School, Bellingham, WA.
18. Howell, P., Blessing, R., Smith, G., and Weeks, C. (2000) Optimizing DREAR and SnB parameters for determining Se-atom substructures, *Acta Crystallogr. D56*, 604−617.

19. Brünger, A. T., Adams, P. D., Clore, G. M., DeLano, W. L., Gros, P., Grosse-Kunstleve, R. W., Jiang, J. S., Kuszewski, J., Nilges, M., Pannu, N. S., Read, R. J., Rice, L. M., Simonson, T., and Warren, G. L. (1998) Crystallography & NMR system: A new software suite for macromolecular structure determination, *Acta Crystallogr. D54*, 905−921.
20. Kleywegt, G. J. (1999) Experimental assessment of differences between related protein crystal structure, *Acta Crystallogr. D55*, 1878−1884.
21. Jones, T. A., Zou, J.-Y., Cowan, S. W., and Kjeldgaard, M. (1991) Improved methods for the building of protein models in electron density maps and the location of errors in these models, *Acta Crystallogr. A47*, 110−119.
22. Martin, A. C. (1998) *ProFit*, version 1.8, SciTech Software, London.
23. Liang, J., Edelsbrunner, H., and Woodward, C. (1999) Anatomy of Protein Pockets and Cavity: Measurement of binding site geometry and implication on ligand design, *Protein Sci. 7*, 1884−1897.
24. Erion, M. D., Takabayashi, K., Smith, H. B., Kessi, J., Wagner, S., Honger, S., Shames, S. L., and Ealick, S. E. (1997) Purine nucleoside phosphorylase. 1. Structure−function studies, *Biochemistry 36*, 11725−11734.
25. Erion, M. D., Stoeckler, J. D., Guida, W. C., Walter, R. L., and Ealick, S. E. (1997) Purine nucleoside phosphorylase. 2. Catalytic mechanism, *Biochemistry 36*, 11735−11748.
26. Kraulis, P. J. (1991) MOLSCRIPT: a program to produce both detailed and schematic plots of protein structures, *J. Appl. Crystallogr. 24*, 946−950.
27. Merritt, E. A., and Murphy, M. E. P. (1994) Raster 3D Version 2.0: A Program for Photorealistic Molecular Graphics, *Acta Crystallogr. D50*, 869−873.
28. Merritt, E. A., and Bacon, D. J. (1997) Raster3D: Photorealistic Molecular Graphics, *Methods Enzymol. 277*, 505−524.
29. Kraulis, P. J. (1991) MOLSCRIPT: a program to produce both detailed and schematic plots of protein structures, *J. Appl. Crystallogr. 24*, 946−950.
30. Esnouf, R. (1997) An extensively modified version of Molscript which includes greatly enhanced colouring capabilities, *J. Mol. Graphics 15*, 132−134.

BI035723K